Biol. Cybern. 52, 45–51 (1985)

Biological Cybernetics

An Overall Description of Retinotopic Mapping in the Cat's Visual Cortex Areas 17, 18, and 19*

Hanspeter A. Mallot

Institut für Zoologie III (Biophysik), Johannes-Gutenberg-Universität, Saarstrasse 21, D-6500 Mainz, Federal Republic of Germany

Abstract. Mathematical functions are derived which model the retinotopic mapping in the cat's visual cortical areas 17, 18, and 19. All three mappings are simple modifications of a complex power function with an exponent of 0.43. This function is decomposed so as to give an intermediate stage which is common to all three mappings and can be regarded as a model of the lateral geniculate nucleus mapping. The influence of retinotopic mapping on visual receptive fields was studied. The results show that a dependence of the receptive field properties on the position in the visual field is to be expected.

1 Introduction

Since the work of Daniel and Whitteridge (1961) on the retinotopic mapping of the visual field in the cortical area V1 of monkeys, a considerable amount of data on receptotopic mapping in different regions of the brain and in a variety of species has been collected. There have also been some attempts to derive a concise mathematical formulation of the retinotopic transformations. The concept of complex logarithmic mapping (Fischer, 1973; Schwartz, 1977) proved to be especially well suited to model the retinotopic distortion in the monkey (cf. Allman and Kaas, 1971; Daniel and Whitteridge, 1961). However, the mapping in the cortical area 17 in the cat (Tusa et al., 1978) resembles the complex logarithmic mapping only poorly. Schwartz (1980) and Epstein (1984) made attempts to reconcile the data of Tusa et al. (1978) with the concept of complex logarithmic mapping, but they only succeeded by treating the upper and lower part of the visual hemifield differently. Furthermore, the decrease of the areal magnification factor at higher eccentricities in the cat does not show the inverse square law that would be predicted for complex logarithmic mapping (cf. Sect. 3.1).

In this paper, a concise description of the retinotopic mapping in the cat's area 17 as revealed by Tusa et al. (1978) is derived. It turns out that simple modifications of the function constructed for area 17 can model even the perimeter charts of areas 18 and 19 (cf. Tusa et al., 1979). The resulting mapping is *not* conformal and therefore complex variables are used only heuristically.

As a first application, the effect of the derived mapping on visual receptive fields is studied in Sect. 6.

2 The Mapping Problem Formalized

The notion of receptotopic mapping means that a point of a neural surface is assigned to each point of a sensoric surface in a continuous way, i.e., retinotopic mapping can be regarded as a continuous or at least piecewise continuous, vector valued function, the domain of which is the visual field. In this paper, the visual field V (i.e., the domain of the function) and its neural representation are treated as subsets of the plane, $\mathbb{R}^2$. The function thus relates a point on a tangent screen in front of the animal with a point on a flat map of a cortical area. It should be clear that this is perfectly equivalent to the mapping of a retinal point onto a point of the folded cortex, since both the relation of a point on the tangent screen to a retinal point and the correspondence between a flat cortical map and the folded cortex are well known. In order to keep the results comparable with the data of Tusa et al. (1978, 1979), mappings are visualized by a parallel projection of a grid of spherical polar coordinates onto a plane (i.e. tangent screen).

* This work is part of the author's doctoral thesis. It was supported by the Deutsche Forschungsgemeinschaft, Grant Se 251/26-1, and by the Stiftung Volkswagenwerk, Grant I/60 511. Professor Dr. W. v. Seelen was in charge of the projects

Besides the actual perimeter charts, magnification factors are particularly useful in studying retinotopic mapping. There is a lot of data on areal magnification relating a given area of the visual field to the area of the corresponding cortical representation. When retinotopic mapping is considered as a function, the areal magnification factor corresponds to the absolute value of the Jacobian of this function.

Let $R: V \to \mathbb{R}^2$, $V \subset \mathbb{R}^2$, denote a retinotopic mapping of the visual field V. The Jacobian J_R of R is then defined as the determinant of R', i.e.,

$$J_R(x, y) := \begin{vmatrix} \partial R_u/\partial x, \partial R_u/\partial y \\ \partial R_v/\partial x, \partial R_v/\partial y \end{vmatrix} = \partial R_u/\partial x \cdot \partial R_v/\partial y - \partial R_u/\partial y \cdot \partial R_v/\partial x, \quad (1)$$

where R_u and R_v denote the components of the vector $R(x, y)$.

It should be noted that the linear magnification factor is not simply the square root of the areal magnification factor. This is only true for conformal mappings. In the more general framework of vector analysis, linear magnification may depend on the direction along which it is measured.

Computations were done in FORTRAN IV on a Nova 3 computer.

3 Construction of an Appropriate Function

It seems rather unlikely that a simple function exists which fits the relativel complicated looking perimeter charts. Therefore, it is necessary to look for a step-by-step approximation. However, there would be little use for a series expansion of the desired function since no neural equivalent of the summation of mappings seems to exist. A step-by-step approximation which can be interpreted in terms of neural systems is the subsequent application of several distortions, such as in the sequence retina – LGN (lateral geniculate nucleus) – area 17. In order to gain insight in retinotopic mappings one should therefore try to find a composition of simple functions matching the data. The following information was used to make a suitable choice of functions.

3.1 Magnification Factors

A satisfactory fit to the data of Tusa et al. (1978) and Albus and Beckmann (1980) on the areal magnification along the horizontal meridian in area 17 is provided by the following power functions:

$$M = cr^{-1.13} \quad \text{(Tusa et al., 1978, Fig. 8)}, \quad (2)$$

$$M = cr^{-1.59} \quad \text{(Albus and Beckmann, 1980, Fig. 15)}. \quad (3)$$

Here, r denotes eccentricity and c is an arbitrary constant. According to the data of Albus and Beckmann, essentially the same power function fits the magnification in the areas 18 and 19, whereas the data of Tusa et al. (1979) indicate that the fit ought to be different in the peripheral parts of area 18. Equation (2) remains valid, however, in the central part of area 18 and in area 19. In the following, (2) is therefore used as a constraint for all three mappings.

In complex logarithmic mapping, the exponent in (2) and (3) is -2; it is therefore excluded from further analysis. The conformal mapping, the Jacobian of which behaves as M in (2) is a complex power function. In general, all mappings for which (2) holds are compositions of this complex power function which an equal-area distortion. It is therefore useful to consider this power function first. Let $R: (x, y) \to (u, v)$ be defined by

$$(u + jv) = (x + jy)^p, \quad (4)$$

where j is the imaginary unit. In real notation we have

$$R: (x, y) \to (u, v) := (x^2 + y^2)^{p/2} \cdot \begin{pmatrix} \cos(p(2n\pi + \arctan y/x)) \\ \sin(p(2n\pi + \arctan y/x)) \end{pmatrix}, \quad (5)$$

where n is a suitable integer. The Jacobian of R can now be readily computed:

$$J_R(x, y) = 2p^2(x^2 + y^2)^{p-1}. \quad (6)$$

From (2) we have $2(p-1) = -1.13$, i.e., $p = 0.43$.

3.2 Topological Constraints

The main difference between the maps of areas 18 and 19 and that of area 17 is that the outer part of the horizontal meridian is represented twice in the former areas. This has been called a field discontinuity by Van Essen et al. (1981). In the complex power function with an exponent less than unity, this behaviour is well known for the left (i.e. negative) part of the real axis. It is due to the ambiguity of the arctan function (5). When approaching the negative real axis from above ($y > 0$), $\arctan(y/x)$ will evaluate to π for negative x, whereas when approaching the axis from below ($y < 0$) it will evaluate to $-\pi$. The complex logarithm, which in real notation requires the arctan, too, shows a similar behaviour. It should be noted, however, that in complex logarithmic mapping the discontinuity is not just a bifurcation of the real axis at zero, but rather the branches of the negative real axis are removed from its positive part.

If the perimeter charts of areas 18 and 19 on the one hand and area 17 on the other are to be described by one function, it would thus be sufficient to mirror the

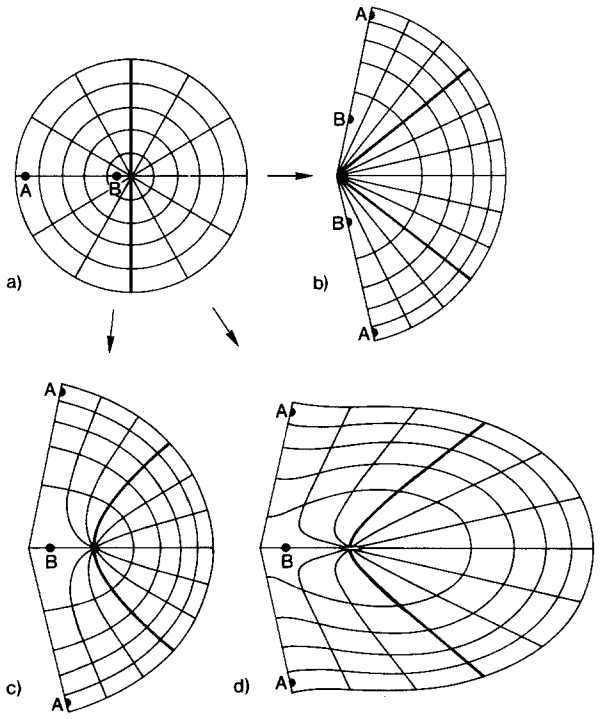

Fig. 1. a Polar grid; **b** transformation of a polar grid by the complex power function (exponent 0.43); **c** by an eccentric power function $R(x+1, y)$; **d** by the two-step-modification $R_2(R_1(x, y) + (1, 0))$. The images of two points on the negative real axis are indicated. In **b** the negative real axis is split throughout, in **c** only the more peripheral part is split, but the point of greatest magnification is removed from the centre of gaze. In **d** both requirements are met

visual hemifield in order to obtain negative coordinates in the precursor of the maps of areas 18 and 19. Figure 1b shows the transformation of the entire visual field by the complex power function ($p=0.43$). The upper and lower left side of the plot may be regarded a first approximation of the area 18 map, bordering on area 17 (right) along the vertical meridian. Figure 1c shows the function $(u, v)=R((x, y)+(1, 0))$ (cf. 5), i.e. an eccentric power function. Here, the horizontal meridian in the left part is divided for larger eccentricities only. However, this leads to a new problem: in the area 18 map in Fig. 1c, magnification is largest not at the area centralis, but at the branch point, where the horizontal meridian forks. It is therefore necessary to separate the part of the function responsible for the magnification from that generating the discontinuity.

This is done by decomposing the function R as defined in (5) into two parts, R_1 and R_2, $R=R_2 \circ R_1$, where "$\circ$" stands for composition. R_1 contains the radial compression responsible for the magnification factor:

$$R_1: (x, y) \to (s, t) = (x, y) \cdot (x^2+y^2)^{(p-1)/2}, \tag{7}$$

R_2 contains the tangential compression, which gives rise to the discontinuity:

$$R_2: (s, t) \to (u, v) = (s^2+t^2)^{1/2} \cdot \begin{pmatrix} \cos(p(2n\pi + \arctan t/s)) \\ \sin(p(2n\pi + \arctan t/s)) \end{pmatrix}. \tag{8}$$

R_2 is equal-area except for a constant $2p$.

Figure 1d shows the transformation of the polar grid obtained by the function $(u, v)=R_2(R_1(x, y) + (1, 0))$, i.e. the shift necessary to keep part of the negative axis undivided is introduced only after the radial compression. Thus, the point of largest magnification has become independent from the branch point. Clearly, the mapping in Fig. 1d is no longer conformal.

The function $R_2(R_1(x, y)+(1, 0))$ appears to be equally suited to model both area 18 and area 19. After all distortions have been performed, the plot has to be mirrored at the vertical axis once more to obtain an area 19 model.

3.3 Additional Equal-Area Distortions

In order to match the perimeter charts published by Tusa et al. (1978 and 1979), additional equal-area distortions were composed with the two steps R_1 and R_2. Although there is a large variety of equal-area mappings, only shifts and linear distortions were used, i.e.:

$$L: \begin{pmatrix} x \\ y \end{pmatrix} \to \begin{pmatrix} u \\ v \end{pmatrix} := \begin{pmatrix} a & b \\ c & d \end{pmatrix} \cdot \begin{pmatrix} x \\ y \end{pmatrix} + \begin{pmatrix} u_0 \\ v_0 \end{pmatrix}. \tag{9}$$

These are the simplest functions that could be chosen; besides shifts, they represent rotations, compressions or extensions of straight lines, and mirroring.

An important point not yet treated is the difference between the mappings in the upper and lower parts of the visual hemifield. It is modelled by the introduction of a linear distortion L_1 prior to the radial compression, R_1. As depicted in Fig. 2 (first step), a linear distortion, though equal-area, may change the distances of symmetric points in the upper and lower part of the hemifield from the centre of gaze. As a consequence, the effect of the radial compression increases with this distance. Thus, in the plot of $R_1 \circ L_1$ (Fig. 2, second step) a difference in the total area covered by the representations of the upper and lower part of the visual hemifield results. It therefore seems reasonable to fit the perimeter charts published by Tusa et al. (1978, 1979) by a composition of the following type:

$$R = R_2 \circ L_2 \circ R_1 \circ L_1. \tag{10}$$

The first two steps, $R_1 \circ L_1$, can be regarded as the LGN mapping (cf. Malpeli and Baker, 1975, for the

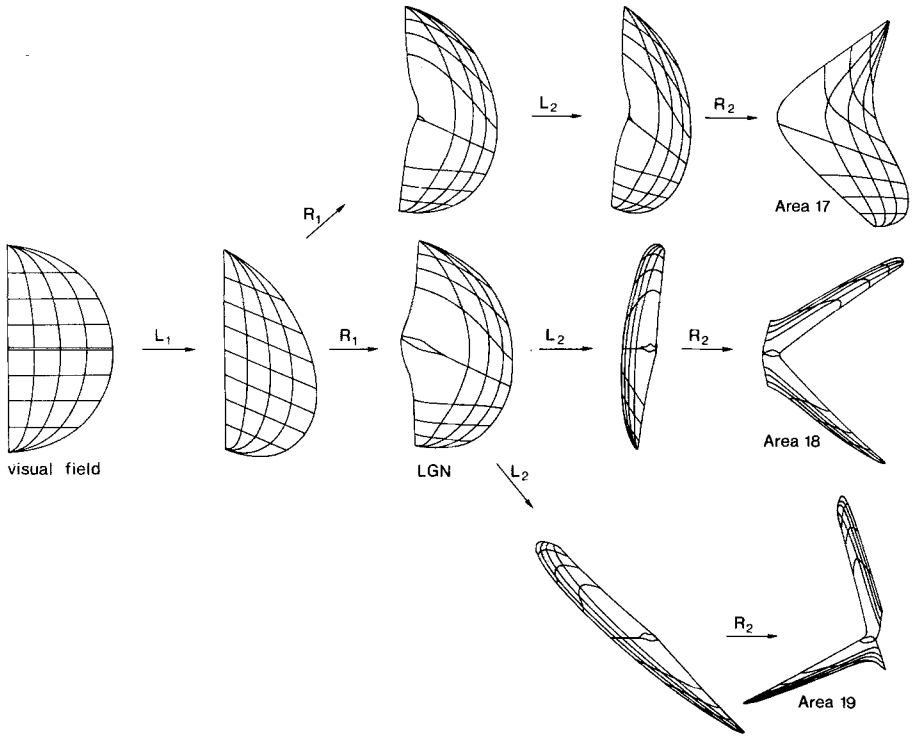

Fig. 2. Formation of the final mapping by the various steps explained in the text. The visual field is represented by a grid of spherical polar coordinates

monkey), which is most probably a common precursor of all three cortical maps.

3.4 Final Model

The final model and the steps leading to it are depicted in Figs. 3 and 2, respectively. Starting with a spherical polar grid for the visual field, a linear distortion is performed as a common step for all three cortical areas. In the path leading to area 17 it is shifted a bit to the right and down, and in the path leading to areas 18 and 19 it is shifted left and up, so that spatial zero remains on the representation of the horizontal meridian.

$$L_1 : \begin{pmatrix} x \\ y \end{pmatrix} \to \begin{pmatrix} u \\ v \end{pmatrix} := \begin{pmatrix} 0.9 & 0.0 \\ -0.4 & -1.0 \end{pmatrix} \begin{pmatrix} x \\ y \end{pmatrix} \pm \begin{pmatrix} 0.18 \\ -0.08 \end{pmatrix}. \tag{11}$$

The shift is added in the path leading to area 17 and subtracted in the one to area 18. Now, function R_1 is applied to the two shifted grids (only one is shown in Fig. 2). The constant p in (7) takes the value 0.43, which fits the magnification data of Tusa et al. (1978). The resulting intermediate stage is essentially common to all three mappings and may be regarded as a model of the LGN map. It exhibits the difference in total area of upper and lower part of the visual hemifield. The decrease in magnification at greater eccentricities is already fully developed and is not altered in the subsequent steps.

The linear distortion L_2, which now follows, essentially contains all differences between the cortical mappings. In the path towards area 17, it deviates only a little from identity and might have been omitted. For the precursors of areas 18 and 19 one has to observe the following constraints: first, the representations of the horizontal meridian in the two grids has to be horizontal with negative orientation in order to make the function R_2 split the more peripheral parts along this meridian. Second, the representations of the vertical meridian in the precursors of areas 17 and 18 and the representations of the horizontal meridian in the precursors of areas 18 and 19 ought to be equal. This is necessary to make the transition from one area to another continuous. The matrices and shifts for the functions L_2 are presented in Table 1.

Finally, the tangential compression, R_2 (8), was performed in all three mappings. With $p=0.43$ in (8), one obtains the results for areas 17 and 18. Since the representation of the horizontal meridian in area 19 borders on the one in area 18, the tangential com-

Table 1. Parameters for the function L_2 in the mappings of areas 17, 18, and 19 [Nomenclature as in (9)]

Area	Matrix				Shift	
	a	b	c	d	u_0	v_0
17	0.7	0.1	−0.2	0.9	0.15	0
18	−0.225	0.1	0.4	0.9	0.15	0
19	−0.534	−0.6	0.267	0.6	0.15	0

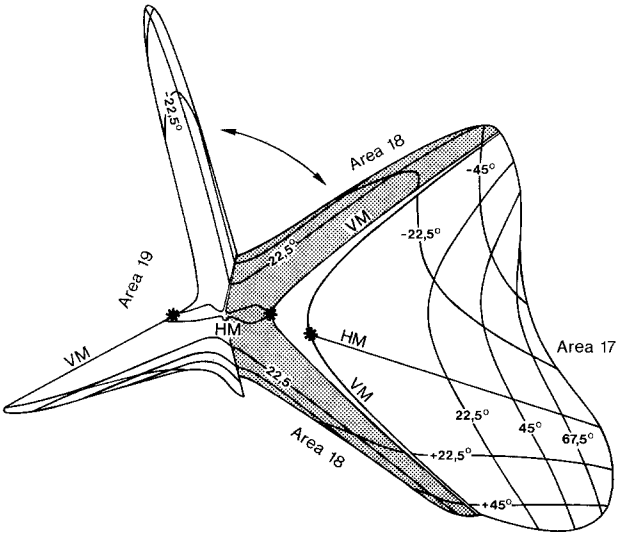

Fig. 3. Final model of the retinotopic mapping in the areas 17, 18, and 19. Those parts of the visual field that are not represented in the brain are omitted. The gaps can be closed in a three-dimensional model

pression has to be somewhat lower here; the appropriate choice for p is $1-0.43=0.57$. As already mentioned in Sect. 3.2, an additional mirroring is required for the map of area 19.

All three perimeter charts are drawn together in Fig. 3. No additional shifts were necessary to make them border on one another. Those parts of the visual field that are not represented in an area according to Tusa et al. (1978, 1979), were omitted. There are two gaps in this map that do not occur in the corresponding figure of Tusa et al. (1979, Fig. 2): first, the most peripheral parts in the lower visual field in areas 18 and 19 should border on one another. This can be obtained in a three-dimensional folding. If the borders of areas 18 and 19 are joined together as indicated by the arrow, a fold results which may be interpreted as the lateral sulcus of the brain. The second gap lies between the representations of the vertical meridian in areas 17 and 18. It can also be closed in a folded map, when area 18 is bent downwards relative to area 17. For this procedure, area 17 should be slightly magnified.

4 Discussion

The presented function differs from previous formalization in two points: first, it uses the complex power function instead of the complex logarithm. The power function fits magnification data (2, 3) and provides an adequate model of the field discontinuity (Van Essen et al., 1981) or second order transformation of the visual field in areas 18 and 19. Second, the mapping finally derived is not conformal due to the composition with linear distortions other than rotations. Although the concept of conformal mapping is largely used in studies on the monkey, there seems to be no theoretical reason why a retinotopic mapping should be conformal. Even if morphogenesis implies a conformal mapping as a solution of some diffusion equation (Schwartz, 1977), it may be concealed in the adult animal by allometric growth of the cortex occurring after the formation of the connections.

For the presence of a linear distortion in the retinotopic mapping of the cat, there is additional evidence from the paper by Epstein (1984), who suggested that the deviation of the cat's mapping from the complex logarithm may be interpreted as a correction of the cat's distorted view of the ground it stands on. This perspective foreshortening is approximately equal to a parallel projection along an oblique line, i.e., a linear distortion. The inverse distortion, which is necessary for the compensation, is linear, too, and actually resembles the mapping L_1 in (11) and Fig. 2.

Linear distortions in the brain can be produced by a very simple mechanism: suppose an orderly organized bundle of nerve fibres meets a sheet of nerve cells at an oblique angle. The resulting mapping would then be an oblique projection, i.e. a kind of linear distortion. Mirroring may be obtained even more easily when a neural surface receives and emits fibres on the same side. Finally, rotations can be constructed as a composition of mirrorings.

In order to obtain the final result of Fig. 3, it is not necessary to perform the steps of the distortion in exactly the same order as depicted in Fig. 2. For example, it is possible to perform the mirroring in L_2 (precursor of areas 18 and 19) in L_1, since the composition of R_1 with mirrorings and rotations is commutative. This, of course, would considerably change the components of the matrices of L_1 and L_2.

In addition to the shift in L_2 (cf. Sect. 3.2), a first shift is already performed in distortion L_1. When a shift is performed only in L_2, as shown in Fig. 1d, a strong correlation exists between the width of area 18 and the curvature of the vertical meridian in area 17. In order to meet both requirements, a narrow area 18 and a smoothly curved vertical meridian in area 17, an additional shift is required in L_1. Then, of course, the point of greatest magnification appears at some distance from the area centralis in the areas 18 and 19. A possible interpretation of this finding is that these areas receive a strong input from retinal Y cells, which are known to be more frequent at a certain distance from the area centralis.

5 Conclusion

Figure 3 shows that it is possible to model the retinotopic mappings in the LGN and the visual areas

17, 18, and 19 by closely related functions. The comprehensive model exhibits the general form of the mappings, the differences between the upper and lower part of the visual hemifield, and the field discontinuity in areas 18 and 19. The areal magnification is generated in the first two steps of the distortion, i.e. in the LGN mapping. This is well in line with the finding that areal magnification is essentially a consequence of the varying ganglion cell density in the retina. It follows that the third and fourth step, leading from the LGN to the cortex, have constant magnification, as have the "mappings" of one cortical area onto another.

The uniformity of the model for the three visual areas is in some contradiction to the largely accepted view that there is a fundamental difference between the mappings in areas 17 and 18, due to the discontinuity in the area 18 map. From the above results it follows that the area 18 map is in some sense a perfectly natural continuation of the area 17 map. Furthermore, there is no need for different models of the representations of the upper and lower part of the visual hemifield in area 17 either.

It is interesting that the differences between the three cortical maps stem from the presence or absence of such simple operations as mirroring or shift (step L_2 of the model), rendering the task of building multiple representations of the visual field a very simple one. Further, one might consider the possibility of neurally performed shifts, which would result in stimulus dependent variations of the retinotopic map. By the same token, the ontogenetic formation of such multiple representations could be governed by only one mechanism or morphogenetic field.

The relationship of the mappings suggests a relation of the functional properties of the three areas. As a first step towards the understanding of such a relation, the influence of the distortion on visual receptive fields is studied in the following section.

6 Appendix

Effect of the Mapping on Visual Receptive Fields

A relatively simple method to investigate the functional relevance of retinotopic mapping is to study its influence on the receptive fields. A receptive field can be formalized by the so-called weighting function, which assigns to each point in the visual field the effect of a stimulus at that point on the cell studied. As a visualization, contour lines of the weighting function are used in Fig. 4.

Suppose the processing in a cortical area can be described by a spatial convolution with a coupling function $k(u, v)$. Let $p(x, y)$ denote a "picture", i.e. a two-dimensional distribution of light; a mapping $R:(x, y)\to(u, v)$ transforms this picture into a cortical input $q(u, v)=p(R^{-1}(u, v))$. Let $e(u, v)$ denote the excitation of a cell at the position (u, v). The convolution then reads:

$$e(u, v)=\int\int q(u', v')k(u-u', v-v')du'dv'. \quad (12)$$

In order to calculate the weighting function from (12), one has to substitute $R(x, y)$ for (u', v'). For fixed (u, v), the kernel of the resulting integral equation models the weighting function of the receptive field:

$$e(u, v)=\int\int p(x, y)k((u, v)-R(x, y))|J_R(x, y)|dxdy. \quad (13)$$

Here, J_R is defined as in (1)

From (13) it follows that the weighting function of the receptive field of a given cell is not just the back-projected cortical coupling function of that cell. Rather, this must be multiplied by the areal magnification at each point. An interpretation of this finding is that the influence of a spot in the visual field on a cortical cell will be the stronger, the larger its representation is.

Figure 4 shows contour lines of a cortical coupling function (4b) and of the associated weighting function of the receptive field (4a). These lines show the points of equal excitation or inhibition imposed on the cell by a suitable stimulus presented at that point. The cortical coupling function chosen is rotationally symmetric, but the resulting receptive fields are clearly oriented and direction specific. This example fits well the data of Payne and Berman (1983), who measured the relation between receptive field properties and their absolute

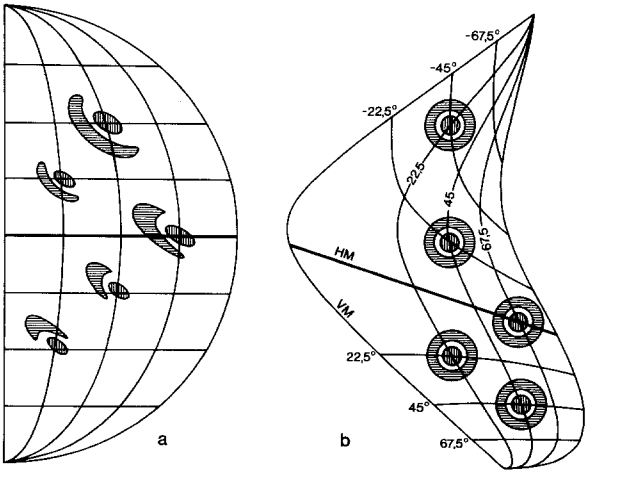

Fig. 4a and b. b Contour lines of a cortical coupling function; **a** the associated weighting function of the receptive field. Intracortical coupling is symbolized by the difference of Gaussian functions. Although cortical coupling is isotropic, a given cell can be influenced most strongly from an asymmetric domain in the visual field. Vertically hatched: more than 30% of maximum excitatory influence; horizontally hatched; more than 70% of maximum inhibitory influence

position in the visual field. They found that orientations at right angles to the direction towards the area centralis are more frequent than oblique ones.

Acknowledgements. I am grateful to Professor Dr. W. v. Seelen and Dr. K. Behrend for helpful discussions on the subject and for critically reading the paper.

References

Albus, K., Beckmann, R.: Second and third visual areas of the cat: Interindividual variability in retinotopic arrangement and cortical location. J. Physiol. (London) **299**, 247–276 (1980)

Allman, J.M., Kaas, J.H.: Representation of the visual field in striate and adjoining cortex of the owl monkey (Aotus trivirgatus). Brain. Res. **35**, 89–106 (1971)

Daniel, P.M., Whitteridge, D.: The representation of the visual field on the cerebral cortex in monkeys. J. Physiol. (London) **159**, 203–221 (1961)

Epstein, L.I.: An attempt to explain the differences between the upper and lower halves of the striate cortical map of the cat's field of view. Biol. Cybern. **49**, 175–177 (1984)

Fischer, B.: Overlap of receptive field centers and representation of the visual field in the cat's optic tract. Vision Res. **13**, 2113–2120 (1973)

Malpeli, J.G., Baker, F.H.: The representation of the visual field in the lateral geniculate nucleus of Macaca mulatta. J. Comp. Neurol. **161**, 569–594 (1975)

Payne, B.R., Berman, N.: Functional organization of neurons in cat striate cortex: Variations in preferred orientation and orientation selectivity with receptive-field type, ocular dominance, and location in visual-field map. J. Neurophysiol. **49**, 1051–1072 (1983)

Schwartz, E.L.: Afferent geometry in the primate visual cortex and the generation of neuronal trigger features. Biol. Cybern. **28**, 1–14 (1977)

Schwartz, E.L.: Computational anatomy and functional architecture of striate cortex: A spatial mapping approach to perceptual coding. Vision Res. **20**, 645–669 (1980)

Tusa, R.J., Palmer, L.A., Rosenquist, A.C.: The retinotopic organization of area 17 (striate cortex) in the cat. J. Comp. Neurol. **177**, 213–236 (1978)

Tusa, R.J., Rosenquist, A.C., Palmer, L.A.: Retinotopic organization of areas 18 and 19 in the cat. J. Comp. Neurol. **185**, 657–678 (1979)

Van Essen, D.C., Maunsell, J.H.R., Bixby, J.L.: The middle temporal visual area in the macaque: Myeloarchitecture, connections, functional properties, and topographic organization. J. Comp. Neurol. **199**, 293–326 (1981)

Received: January 24, 1985

Hanspeter A. Mallot
Institut für Zoologie III (Biophysik)
Johannes Gutenberg-Universität
Saarstrasse 21
D-6500 Mainz
Federal Republic of Germany